Correlations in the interface structure of Langmuir-Blodgett films observed by x-ray scattering

V. Nitz, M. Tolan, J.-P. Schlomka, O. H. Seeck, J. Stettner, and W. Press
Institut für Experimentalphysik, Christian-Albrechts-Universität Kiel, Olshausenstraβe 40-60, 24098 Kiel, Germany

M. Stelzle and E. Sackmann
Technische Universität München, Physik Department E22, 85748 Garching, Germany
(Received 27 November 1995; revised manuscript received 23 February 1996)

X-ray scattering experiments within the region of total external reflection as well as grazing-incidence-diffraction measurements from Langmuir-Blodgett films are shown. All measurements are explained quantitatively using the distorted-wave Born approximation (small q_z regions) or a simple kinematic scattering theory (large q_z regions) for layered systems. Since rather imperfect systems are investigated, strong vertical correlations between the roughnesses of the organic layer interfaces were found for two samples consisting of 9 and 11 layers, respectively, of cadmium-arachidate on silicon (100) surfaces. This conformal roughness does not stem from the substrate but from defects and holes of the first transferred layer. The model of self-affine rough interfaces yields consistent parameters compared with grazing incidence diffraction experiments and no hints towards a cadmium-arachidate island formation are observed. [S0163-1829(96)07331-6]

I. INTRODUCTION

Organic multilayers currently play an important role in thin-film technology research. Possible applications for these films are coatings of glass fibers for light transmission, high speed optical control elements in microelectronics, improvement of surface quality of mirrors, and detectors for organic molecules as biosensoric devices.[1–3] In analogy to the molecular-beam-epitaxy (MBE) layer-by-layer growth of semiconductor materials, the Langmuir-Blodgett (LB) technique[4] can be used to prepare organic multilayers of well-defined thickness and composition. These layers are transferred to a solid substrate, e.g., a silicon wafer, from the liquid subphase by repeating a simple dipping procedure. This technique leads one to expect that imperfections will be transferred completely from one layer to the next. In this paper we focus on this special topic of correlated or conformal roughness in LB films, which is of decisive importance for the preparation of high-quality organic multilayers.

Whereas the structure and phase transitions of Langmuir films on water surfaces have been the focus of many works during the last decade (for a review see Als-Nielsen *et al.*[5]), the detailed lateral structure of LB films on solid substrates is less understood. Only a few diffuse x-ray scattering studies of this topic exist.[6–8] Since the diffuse scattering theory for layered systems was worked out in great detail during the last two years (see below) now a more quantitative description of the interface structure of LB films becomes possible. Questions concerning the degree of conformality of the organic layers, the detailed morphology of the interfaces, and the possible evolution of the roughness from the substrate to the top layers (smoothing or amplifying tendencies) will be addressed in our study. Recently Gibaud *et al.*[9] have found evidence of self-affine rough interfaces in a LB film. This important result leads one to suspect that even in systems consisting of ''pencil-like'' molecules a certain amount of disorder exists so that statistical models are applicable for a new class of interfaces. The aim of the present work is to shed some more light on this point in connection with the above-mentioned roughness correlations.

It is well known that x-ray scattering is a powerful and nondestructive probe for investigating thin films. X-ray reflectivity has become a common tool for determining density profiles of thin films and multilayers.[10–15] The nonspecularly scattered diffuse intensity, on the other hand, is mainly sensitive to the lateral structure of rough interfaces, in particular to the respective height-height correlation functions. The diffuse scattering cross section of a single surface was calculated using the distorted-wave Born approximation (DWBA).[16–18] Later these results were extended to layered systems including the effect of vertical correlations between the interfaces.[19,20] Recently it was shown that diffuse x-ray scattering data from evaporated Si/Ge and MBE $CoSi_2$ layers can be quantitatively explained using the DWBA on the basis of a particular data analysis.[21–23]

In this paper we present x-ray scattering experiments on two LB samples. It is shown that the LB preparation technique yields highly correlated interface structures. After the Introduction, the scattering theory and a discussion of correlation functions are briefly presented. Then a description of the sample preparation and the experimental setup follows. Furthermore the measurements and the corresponding fits are shown and compared with the results of grazing incidence diffraction (GID) investigations. A discussion, conclusions, a summary, and an outlook finish this paper.

II. SCATTERING THEORY

A. Specular reflectivity

We assume a sample consisting of N layers $j=1,\ldots,N$. The refractive index n_j of layer j is $n_j=1-\delta_j+i\beta_j$ with the dispersion δ_j and the absorption β_j. Then the Fresnel-reflection and -transmission coefficients for each (smooth) interface are $r_{j,j+1}=(k_{z,j}-k_{z,j+1})/(k_{z,j}+k_{z,j+1})$ and $t_{j,j+1}=2k_{z,j}/(k_{z,j}+k_{z,j+1})$, respectively,[24] with $k_{z,j}$ the z component of the wave vector in medium j, which is deter-

mined by the law of refraction: $k_{z,j}=k_i(n_j^2-\cos^2\alpha_i)^{1/2}$. Throughout this paper the z axis is directed perpendicular to the surface, x is the lateral direction in the scattering plane, and y denotes the out-of-plane direction. The glancing angle of incidence is α_i and $k_i=k_f=2\pi/\lambda=k_1$ is the modulus of the incoming wave vector (λ is the x-ray wavelength).

The ratio X_j of the amplitudes R_j and T_j of the outgoing to the incoming electromagnetic waves in layer j, which lies between the positions z_{j+1} and z_j (layer thickness $d_j=z_{j+1}-z_j$), can be calculated with the well-known Parratt recurrence relation:[10,24]

$$X_j:=\frac{R_j}{T_j}=e^{-2ik_{z,j}z_j}\,\frac{r_{j,j+1}+X_{j+1}e^{2ik_{z,j+1}z_j}}{1+r_{j,j+1}X_{j+1}e^{2ik_{z,j+1}z_j}}. \qquad (1)$$

If a semi-infinite substrate is assumed, $R_{N+1}=0$ follows and the reflected intensity I is obtained with Eq. (1) via $I=I_0|R_1|^2$. The amplitude of the incoming x-ray wave was set to $T_1=1$.

The recurrence formula (1) not only works for simple layer systems but also for arbitrary electron density profiles $\zeta(z)$. For this purpose the profile has to be sliced into very thin layers of uniform density. The accuracy and the amount of computation time of this method are then determined by the number of layers that are used to approximate the actual density profile.

Small roughnesses (compared with the respective layer thickness) of the interfaces can be included in the description in another way. In this case the Fresnel reflectivities $r_{j,j+1}$ for smooth interfaces are replaced in Eq. (1) by the coefficients $\tilde{r}_{j,j+1}$ for rough interfaces. An analytical solution can be found for the tanh-refractive index profile between layer j and $j+1$ leading to the expression[13,25,26]

$$\tilde{r}_{j,j+1}=\frac{\sinh[(\pi/2)^{1.5}\sigma_j(k_{z,j}-k_{z,j+1})]}{\sinh[(\pi/2)^{1.5}\sigma_j(k_{z,j}+k_{z,j+1})]}\,G(\sigma_j,k_{z,j},k_{z,j+1}).$$

The factor $G(\sigma_j,k_{z,j},k_{z,j+1})$ is always set to 1 in the case of hard x rays and roughnesses up to $\sigma_j\approx 100$ Å.[27] It is important to mention that the tanh profile is very similar to an error-function profile with a Gaussian probability density and root-mean-square (rms) roughness σ_j (Ref. 28) because for the explanation of the diffuse scattering data a Gaussian probability density has to be assumed.[16,19]

B. Diffuse scattering

Lateral information about the interfaces of a layer system can be obtained by analyzing the diffuse nonspecularly scattered intensity. Whereas in principle the calculation of the reflected intensity is exact (solution of the Helmholtz equation with the Parratt formalism, see Sec. II A), the diffusely scattered intensity can only be calculated using various kinds of approximations. In the case of hard x rays and glancing angles of incidence and exit α_i and α_f, respectively, the formulation of the DWBA is used. The roughnesses lead to a nonzero probability for a transition from a state with wave function $|\Psi_i\rangle$ to a wave function $|\Psi_f\rangle$ with $\mathbf{k}_i\neq\mathbf{k}_f$, which means that the interface roughnesses cause all nonspecular scattering contributions. A calculation of the transition matrix elements finally leads to the following expression for the cross section $d\sigma/d\Omega$ of the diffuse scattering (for details see Refs. 19, 20, and 29):

$$\left(\frac{d\sigma}{d\Omega}\right)_{\text{diff}}=\frac{\mathcal{G}k_1^2}{8\pi^2}\sum_{j,k=1}^{N}(n_j^2-n_{j+1}^2)(n_k^2-n_{k+1}^2)^*\sum_{m,n=0}^{3}\tilde{G}_j^m\tilde{G}_k^{n*}\exp\left\{-\frac{1}{2}[(q_{z,j}^m\sigma_j)^2+(q_{z,k}^{n*}\sigma_k)^2]\right\}\mathcal{S}_{jk}^{mn}(q_x,q_{z,j}^m,q_{z,k}^n), \qquad (2)$$

with the structure factor

$$\mathcal{S}_{jk}^{mn}(q_x,q_{z,j}^m,q_{z,k}^n)=\frac{1}{q_{z,j}^m q_{z,k}^{n*}}\int_0^\infty[\exp\{q_{z,j}^m q_{z,k}^{n*}C_{jk}(x)\}-1]\cos(q_x x)\,dx. \qquad (3)$$

Due to the rather coarse resolution perpendicular to the scattering plane, an integration over the out-of-plane wave vector transfer q_y was already performed to obtain Eq. (3). The lateral roughness structure of the interfaces in the x direction is taken into account by the autocorrelation functions $C_j(x)=C_{jj}(x)$ and the corresponding cross-correlation functions $C_{jk}(x)$ between interfaces j and k. The illuminated area of the sample is denoted by $\mathcal{G}$, $\mathbf{q}_j^m=(q_x,q_{z,j}^m)^T$ is the momentum transfer within each layer, and dynamical effects are taken into account by the factors $\tilde{G}_j^m=G_j^m\exp(-iq_{z,j}^m z_j)$. The respective expressions for G_j^m and $\mathbf{q}_j^m$ can be found in the papers of Holý *et al.*[19,20] or Schlomka *et al.*[21] Note that a Gaussian probability density of all roughness distributions was assumed to obtain Eqs. (2) and (3).

C. Correlation functions

Interface roughness is characterized by two quantities: The vertical width σ (rms roughness) and the particular lateral structure. Since the x-ray beam averages over the coherently illuminated area (several micrometers) a statistical description of the lateral structure via correlation functions is straightforward. For interface j at the vertical position $z_j(\mathbf{R})=z_j+\phi_j(\mathbf{R})$ the height-height (auto) correlation function $C_j(\mathbf{R})$ is defined by

$$C_j(\mathbf{R}):=\langle\phi_j(\mathbf{r})\phi_j(\mathbf{r}+\mathbf{R})\rangle_{\mathbf{r}}.$$

Here $\mathbf{R}=\mathbf{r}-\mathbf{r}'$, $\mathbf{r}=(x,y)^T$, and $\mathbf{r}'=(x',y')^T$ are vectors within the surface and $\langle\,\rangle_{\mathbf{r}}$ means the average over the (x,y)

plane. The function $\phi_j(\mathbf{R})$ is the height fluctuation of the interface j, which has the average height z_j and the lateral position $\mathbf{R}$. The rms roughness then is $\sigma_j=\sqrt{C_j(0)}$; the mean value $\langle\phi_j(\mathbf{r})\rangle_{\mathbf{r}}$ of the fluctuating part vanishes.

It has turned out that for many isotropic solid surfaces, $C_j(\mathbf{R})$ can be represented by the correlation function of a self-affine fractal surface:[16,30–33]

$$C_j(R)=\sigma_j^2 e^{-(R/\xi_j)^{2h_j}}, \tag{4}$$

with a lateral cutoff (correlation) length ξ_j and the Hurst parameter h_j.[34–36] The quantity ξ_j describes the length scale on which the interface begins to look rough: For $R<\xi_j$ the surface is self-affine rough whereas for $R>\xi_j$ the surface looks smooth. The Hurst parameter h_j is restricted to the region $0<h_j\leqslant 1$ and defines the fractal box dimension $D_j=3-h_j$ of the interface.[34] Small values of h_j describe jagged surfaces while $h\approx 1$ leads to interfaces with smooth hills and valleys.[16,21,30]

In the present work the fractal correlation function defined by Eq. (4) is taken for all interfaces. This function was introduced to describe semiconductor or metal surfaces. As already mentioned in the Introduction, Gibaud *et al.*[9] were able to explain their data assuming self-affine rough interfaces in LB films. Our investigations strongly support this finding (see Sec. V B). Nevertheless, other correlation functions might be more appropriate. Stömmer *et al.*[6,7] propose a model where single molecules of one layer are arranged laterally in domains. This domain model has the advantage that the microscopic structure is easily included in the theory. Another ansatz for the microscopic structure of LB films of polymers was given by Feigin and Samoilenko.[37] Their slab model is able to explain some features of the diffuse scattering but a dynamic treatment of the scattering from LB films on the base of these models has not yet been achieved.

It is important to note that an x-ray scattering experiment does not yield $C_j(\mathbf{R})$ directly but the respective structure factor [see Eq. (3)]. For small q_z values and small roughnesses σ_j the exponential in the structure factor can be expanded and yields directly the Fourier transform of the correlation function, termed the power spectral density.[19,21,38]

In the past four years, a large body of work has been published concerning correlated or conformal roughness.[39–46] It turns out that a transfer of an imperfection to the next layer seems to be nearly unavoidable and that preparation techniques such as MBE yield samples with a very high degree of vertical roughness correlations.[23]

Vertical correlations between different interfaces j and k are statistically described by cross-correlation functions,

$$C_{jk}(\mathbf{R}):=\langle\phi_j(\mathbf{r})\phi_k(\mathbf{r}+\mathbf{R})\rangle_{\mathbf{r}}.$$

It is quite clear that in general vertical correlations between the interfaces at the positions z_j and z_k should be a function of the spatial roughness frequency.[47–49] Therefore we have used two models for the cross-correlation functions:

(i) The diffusely scattered intensity of the first sample (9-layer LB film) was calculated with the ansatz[21]

$$C_{jk}(R)=\frac{\sigma_j\sigma_k}{2}\left[e^{-(R/\xi_j)^{2h_j}}+e^{-(R/\xi_k)^{2h_k}}\right]e^{-|z_j-z_k|/\xi_{\perp,jk}}, \tag{5}$$

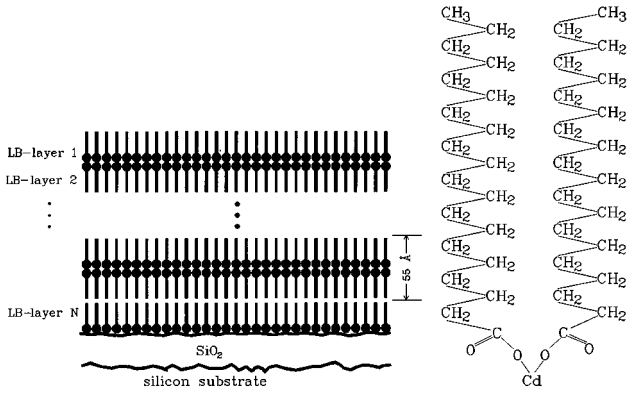

FIG. 1. Left: LB film on a Si/SiO_2 substrate. The Y structure with the characteristic distance of 55 Å between the Cd bilayers is shown. Right: sketch of the cadmium-arachidate (CdA) molecule.

using *different* ξ_j and h_j for each interface. The length $\xi_{\perp,jk}$ is the vertical distance over which the correlations between layers j and k are damped by a factor of $1/e$. No correlations are present in the case $\xi_{\perp,jk}=0$. Nearly perfect correlation means that $\xi_{\perp,jk}$ is much larger than the respective layer thickness $|z_j-z_k|$. In this work, a single parameter $\xi_\perp$ for all vertical correlation lengths $\xi_{\perp,jk}$ was used. To decrease the number of free parameters and to model a simple roughness evolution the values of the parameters σ_j, ξ_j, and h_j of the LB interfaces were linearly interpolated between the first and last layers (see Sec. V B).

(ii) Since the results for the first sample reveal only weak evidence for a roughness evolution inside the LB film (see Sec. V B 1) the data of the second sample (11-layer film) were explained with the cross-correlation function[33,40,41]

$$C_{jk}(R)=\sigma_j\sigma_k e^{-(R/\xi)^{2h}}e^{-|z_j-z_k|/\xi_\perp}, \tag{6}$$

and fixed values ξ and h of the lateral roughness parameters for *all* interfaces of the LB film. Equation (6) means a strong restriction because the replication of the roughness is now independent of the spatial frequency (constant $\xi_\perp$) (Ref. 50) and no lateral roughness evolution is allowed.

III. SAMPLE PREPARATION

Two cadmium-arachidate (CdA) LB films consisting of 9 and 11 layers, respectively, were prepared on Si(100) wafers (see Fig. 1). First a Langmuir trough (for the detailed experimental setup see Ref. 51) was filled with ultraclean water and afterwards a monolayer of the CdA molecules was spread on the surface. Their polar Cd head groups are lying on the water surface and the unpolar hydrocarbon chains are directed outwards. Right after the spreading of the CdA molecules onto the water surface no in-plane order is present. Increasing the lateral pressure Π by decreasing the area of the CdA molecules with a step motor driven barrier leads to a decrease of the intermolecular distances. Depending on the molecular interactions a great variety of phases may occur.[52–54] For $\Pi>25.9$ mN/m a crystalline ordered phase occurs. Only the crystalline phase can be transferred to a solid substrate. During the compression of the CdA monolayer, the surface tension was monitored with a Wilhelmy balance.[55,56] The crystalline phase was indicated by a rapid

TABLE I. Results of the fits for the nine-layer CdA LB film. The first column shows the layer and the respective interface. Values in brackets were not varied during the fit. Note that the parameters σ, ξ, and h of the interfaces 3–5 are connected with a linear interpolation to the parameters of the interfaces 2 and 6 [see Fig. 4(a), the CH-chain/air interface is denoted by number 1].

Layer/interface	d_j (Å)	$\delta_j \times 10^6$	σ_j (Å)	ξ_j (Å)	h_j
Si/SiO_2	(∞)	(7.56)	5±3	600±400	(0.5)
SiO_2/Cd	16±4	5.6±0.5	3.0±1.0	700±200	0.4±0.1
Cd/(int. 6)	1.7±0.5	11.0±2	3.6±1.0	390±120	0.25±0.05
Cd/(int. 2)	2.4±0.5	9.0±1	3.2±1.0	340±100	0.5±0.2
CH chains	53±1	2.8±1.0			
CH-chain/air	20±8	2.4±1.0	15±5	400±200	0.3±0.1
		$\xi_\perp$=700 Å±200 Å			

change in the observed surface tension as a function of the film area.

Before transferring the films on the Si substrates, a procedure using ultraclean water and a subsequent drying in an oven at 100 °C was applied to clean and thin the native oxide layer. Time-dependent specular reflectivity measurements show that the oxide layer was totally removed right after the cleaning and a stable SiO_2 film with a thickness of about $d \approx 16$ Å builds up with a time constant of $\tau \approx 90$ h.[51,57] After the time $t \gg \tau$ the oxide layer thickness remains constant. Whereas the Si/SiO_2 interface of both samples is rather smooth, the roughnesses of the oxide layers are quite different (σ_{oxid}=3 and 12 Å, see Tables I and II). A reason for this might be that the two substrates originate from different wafers. Specular reflectivity measurements have shown that these uncleaned wafers were covered by nonuniform layers of rather large roughness. Obviously the cleaning procedure to remove these layers has corroded the surface of the second substrate much more. However, the fact that the roughnesses of both substrates are quite different has opened the possibility to check whether the LB film is able to smooth a vertical roughness or whether observed roughness correlations are only stemming from replicated imperfections of the internal layer structure of the adsorbed molecules.

The transfer of the LB films was done by a simple dipping technique moving a Si wafer up and down. While the layers are transferred the lateral pressure is kept constant by moving the barrier. This guarantees that the crystalline phase is always present during the sample preparation. Because the bare Si/SiO_2 wafer is a hydrophilic substrate, the polar Cd heads of the CdA molecules are lying on the SiO_2 surface after the first transfer. Then the second layer is transferred with its hydrophobic part, i.e., the carbon chains, on top of the first one. Now the polar Cd heads are directed outwards and every further transfer will produce a layer stack with alternating orientation of the CdA molecules in the above-mentioned manner (see Fig. 1).

With this technique the two investigated CdA LB films consisting of 9 and 11 layers, respectively, are prepared. The particular structure of the layer system that is caused by the

TABLE II. Results of the fits for the 11-layer CdA LB film. The first column contains the layer and respective interface. Values in brackets were not varied during the fit. Note that the parameters ξ and h are assumed to be equal for all LB film interfaces. In the low-density regions only the roughnesses were varied; the dispersion, thicknesses, Hurst parameters, and correlation lengths of the regions (a) to (e) were assumed to be equal [see Fig.4(b)].

Layer/interface	d_j (Å)	$\delta_j \times 10^6$	σ_j (Å)	ξ_j (Å)	h_j
Si/SiO_2	(∞)	(8.79)	1.5±0.3	(1000)	(0.5)
SiO_2/Cd	16±4	6.2±0.3	12.0±0.3	(1000)	(0.5)
Cd/CH-chain	6.0±0.5	10.1±0.6	2.75±0.5	235±30	0.77±0.03
CH-chain/[int. (a)]	24.8±0.2	4.4±0.7	4.0±0.5	235±30	0.77±0.03
Low-density regions					
(a)			4.1±0.4		
(b)			6.9±0.6		
(c)	2.80±0.05	0.03±1.0	5.3±0.5	235±30	0.77±0.03
(d)			4.1±0.3		
(e)			3.8±0.3		
CH-chain/Cd	26.6±0.1	7.1±2.0	7.1±0.5		
Cd/CH-chain (top)	1.5±0.2	16.5±2.0	3.2±0.2		
CH-chain(top)/air	23.3±0.3	5.1±0.7	3.8±0.4		
		$\xi_\perp$=9000 Å±3000 Å			

hydrophobic-hydrophilic head-chain structure of the CdA molecule is called *Y* type. Therefore both investigated samples are *Y*-type CdA LB films.

IV. EXPERIMENTAL SETUP AND SCATTERING GEOMETRY

A. Setup

The x-ray experiments were performed both (i) using a 12-kW rotating anode generator (Rigaku Ru 200) with copper target and a three-crystal diffractometer[51,58] and (ii) at the wiggler beamline W1 at HASYLAB, Hamburg.[14,59]

The x rays from the copper target of the rotating anode generator were collimated by a first slit. Then a Ge(111) monochromator selects the characteristic Cu $K\alpha$ lines from the spectrum. A second slit only picks out the Cu $K\alpha_1$ line with a wavelength of $\lambda=1.54056$ Å, which impinges onto the sample. The accuracy of the step motors, which control the incidence angle α_i and the scattering angle $\Phi:=\alpha_i+\alpha_f$, is 0.001°. The detector unit contains a Ge(111) analyzer and a third slit in front of a NaI(Tl) (Canberra) scintillation counter. Vacuum tubes as well as lead shields around the system were installed to increase intensity and to reduce background radiation (for details see Refs. 51 and 58). The resolution in the region of small incidence and exit angles within the scattering plane is $\delta_{q_x}\approx 2q_z\times 10^{-4}$ and $\delta_{q_z}\approx 7\times 10^{-4}$ Å^{-1} parallel and perpendicular to the surface. The detector is wide open in the out-of-plane direction, which means that the resolution δ_{q_y} is rather coarse [integration over q_y, see Eq. (3)].

The GID experiments and the diffuse scattering measurements from the 11-layer sample were performed at the experimental station ROEWI at beamline W1 at HASYLAB (for a detailed description see Ref. 59). Here a 32 pole wiggler is the x-ray source. The synchrotron radiation impinges onto a Si(111) double-crystal monochromator and afterwards on a gold mirror to suppress higher-order harmonics. For the diffuse scattering measurements the x-ray beam was collimated by two slits of the size 0.5×2 mm^2 in front of the sample to determine the incident angle α_i and two slits of the same size in front of the detector to define the exit angle α_f, respectively. The obtained resolution in the region of total external reflection then is $\delta_{q_x}\approx q_z\times 10^{-3}$ and $\delta_{q_z}\approx 4\times 10^{-3}$ Å^{-1}. Again a NaI(Tl) (Canberra) scintillation counter was used for the diffuse scattering experiments. The GID experiments were done with a position sensitive detector (Braun). To get a better resolution for the GID experiments the widths of the slits in front of the sample were decreased to 0.5×1 mm^2. This yields a resolution of $\delta_\phi\approx 0.07°$ in the direction of a GID detector scan. For all synchrotron measurements a wavelength of $\lambda=1.659$ Å was used.

B. Scattering geometry

Figure 2 shows the paths of the various scans in reciprocal space within the scattering plane. The momentum transfer $\mathbf{q}=\mathbf{k}_f-\mathbf{k}_i=(q_x,0,q_z)^T$ is given by $q_x=k_i(\cos\alpha_f-\cos\alpha_i)\approx k_i/2(\alpha_i-\alpha_f)\Phi$ and $q_z=k_i(\sin\alpha_f+\sin\alpha_i)\approx k_i\Phi$ (see Fig. 3). Therefore a reflectivity ($\alpha_i=\alpha_f$) corresponds to a q_z scan with $q_x=0$. A rocking scan is performed by rotating the sample at a fixed detector position. Thus the incidence angle α_i varies and the scattering angle $\Phi=\alpha_i+\alpha_f$ is constant. Rocking scans are (nearly) q_x scans at a fixed q_z position. By performing a detector scan, which means a scan with fixed angle of incidence α_i and varying scattering angle Φ, the q_x and q_z components of the scattering vector are changed simultaneously. The path of this scan in reciprocal space is a parabola (see Fig. 2). A longitudinal diffuse scan is a near-specular scan. The incidence angle α_i is slightly out of the specular condition, i.e., $\alpha_i-2\delta\alpha_i=\alpha_f$. In reciprocal space this scan lies on a straight line, which is inclined at an angle $\delta\alpha_i$ against the q_z direction. All four different scan modes were performed during the measurements of the two LB samples. Due to geometrical restrictions, the marked area in Fig. 2 is not accessible with the experimental setup of an in-plane diffuse scattering experiment. The GID experiments also include an out-of-plane momentum transfer q_y and the marked area now can be accessed by these scans.

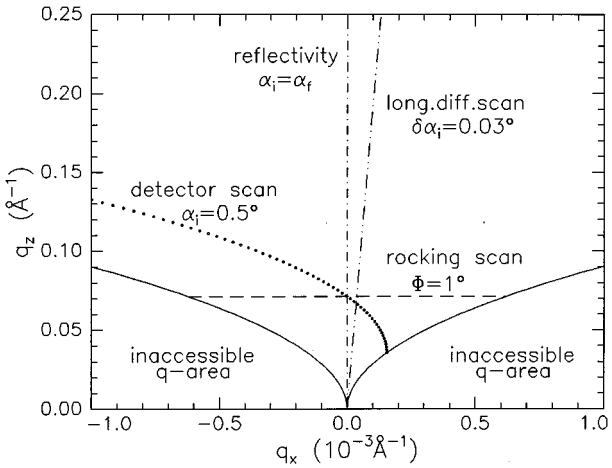

FIG. 2. Scans in reciprocal space (q_x,q_z). The region below the solid line is not accessible with the setup of this work. The dashed line is a rocking scan with a scattering angle $\Phi=\alpha_i+\alpha_f=1°$. The dashed-dotted line represents a reflectivity ($\alpha_i=\alpha_f$, $q_x=0$) and the inclined dashed-dotted line is a longitudinal diffuse scan with an offset $\delta\alpha_i=0.03°$. The path of a detector scan with incidence angle $\alpha_i=0.5°$ is given by the dotted line.

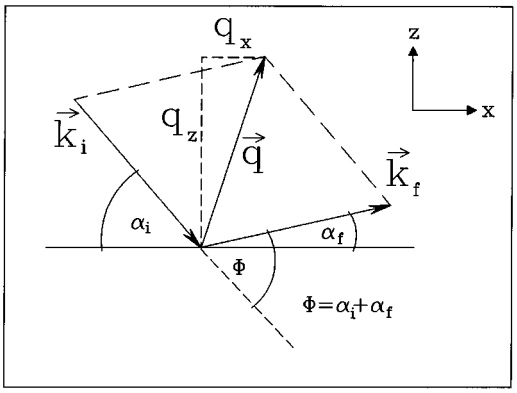

FIG. 3. Scattering geometry. The wave vectors of the incident and scattered x rays are $\mathbf{k}_i$ and $\mathbf{k}_f$, with the incidence and exit angle α_i and α_f, respectively, and the scattering angle Φ. The momentum transfer is defined by $\mathbf{q}=\mathbf{k}_f-\mathbf{k}_i=(q_x,q_z)^T$.

V. MEASUREMENTS, RESULTS, AND DISCUSSION

A. Data analysis

A procedure that is widely used to analyze x-ray reflectivity data is subtracting an off-specular longitudinal diffuse scan from the measurement and refining the obtained true specular data[16] using the models described in Sec. II A. The resultant reflectivity is taken to yield the average density profile $\varrho(z)$ of the sample (layer thicknesses, rms roughnesses). We also analyze our data in this way as a first step to check the layer structure of the LB films, particularly to confirm the characteristic Y-type structure (Fig. 1).

In a second step, the diffusely scattered intensity is included in the analysis. The reflectivity, i.e., the whole intensity for $\alpha_i=\alpha_f$, and the diffuse scattering (several rocking curves, detector, and longitudinal diffuse scans) were measured and fit simultaneously. A detailed description of this data analysis technique is given by Schlomka *et al.*[21] and Stettner *et al.*[23] To obtain estimates for the errors, the fit parameters were changed manually until significant deviations between measurement and calculation occur.

The calculation of the full expression for the diffuse scattering cross section given by Eqs. (2) and (3) is very time consuming. Therefore we used two major approximations: (I) For small q_z values and small roughnesses, the exponential in the integral of Eq. (3) was replaced by the first two terms of its Taylor series. Then the integral is the power spectral density and a very effective computation of Eq. (2) becomes possible. Simulations show that $|q_z\sigma|\approx 1$ is a realistic limit for the validity of this approximation.[23] (II) For large q_z values Eqs. (2) and (3) reduce to the kinematical approximation (simple Born approximation) for multilayers (see, e.g., Sanyal *et al.*[40] or Phang *et al.*[44]). Because all G_j^m factors in Eq. (2) can be set to one or zero, respectively, again an effective computation of the diffuse scattering is achieved. But the region of very small incidence and exit angles, where dynamical effects dominate the scattering, has to be excluded from the analysis.

B. Measurements and fit results

The following slab model is used for the vertical structure of the LB films [see Figs. 4(a) and 4(b)]. The CdA molecule was divided into two slabs of constant electron density: The Cd head group is slab number 1 and the two hydrocarbon chains are slab number 2 (Fig. 1). The touching Cd head groups were combined to regions with uniform electron densities. Between the hydrocarbon chains of each layer a low-density region was introduced to model the intermediate region of the two bilayers [see Fig. 4(b)]. Furthermore between single slabs, rms roughnesses were assumed to smear out the density profile. To reduce the number of free fit parameters, the same thicknesses and electron densities were used for layers of equal composition.

An evolution of the roughness from the bottom to the top was taken into account in the following manner: The vertical rms roughness σ_j and the lateral parameters ξ_j and h_j of each interface were determined by a linear interpolation formula from the values of the first and last LB layers. If $p\in[\sigma,h,\xi]$ is a roughness parameter then the respective value p_j of the jth interface is calculated via $p_{N-j}=p_N+(p_2-p_N)j/(N-2)$ with $j=0,\ldots,N-2$. Therefore the structure of $N-1$ interfaces is described by only six free parameters σ_2,h_2,ξ_2 and $\sigma_N,h_N\xi_N$. A linear increase was chosen for simplicity. More realistic models yield power laws with certain growth exponents (see, e.g., Ref. 60).

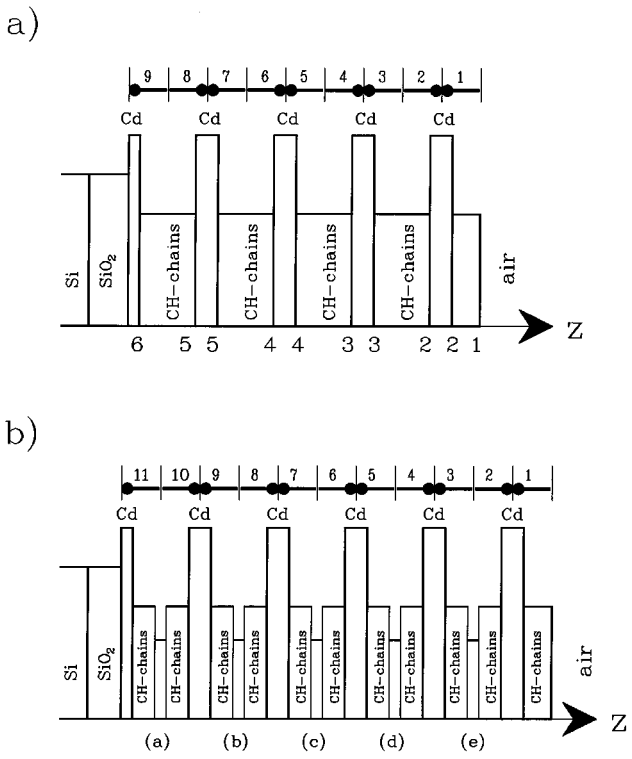

FIG. 4. Density profiles for the fits of the data: (a) The slab model that was used to fit the data of the nine-layer LB film. The Cd bilayers and the bilayers of the CH chains were assumed as slabs with uniform electron density. The numbers at the bottom give the respective numbers of the interfaces that were varied in the fit. Note that for the top and bottom of the thin Cd bilayers the same roughness parameters are assumed (perfect correlation). (b) Slab model for the fit of the 11-layer CdA LB film. Because of the wide q region of the measurement the fit is sensitive to thin regions (a) to (e) of lower electron density between the touching hydrocarbon chains.

1. LB film with 9 layers

The first investigated sample is the LB film with 9 CdA layers. All measurements were done with the rotating anode laboratory source.

The total reflectivity was measured to a wave vector transfer of $q_z=1.4$ Å^{-1}. It turns out that the reflected intensity in the region $q_z>0.7$ Å^{-1} is purely diffuse. Figure 5 shows the true specular intensity (open circles), which was obtained after subtracting an off-specular longitudinal diffuse scan with $\delta\alpha_i=0.05°$. The distance $\Delta q_z=0.113$ Å^{-1} between the Bragg peaks corresponds to the Cd-Cd distance of $2\pi/\Delta q_z=55$ Å, i.e., to the thickness of one bilayer. This is a direct proof of the Y structure of the CdA LB film (see Sec. III). The rapid oscillations ($\Delta q_z=0.025$ Å^{-1}), which correspond to a length of $d=251$ Å, are caused by the total thickness of the layer system. The line in Fig. 5 is a fit to the data with a density profile, which is shown in the inset. Note that this fit was not obtained on the base of a slab model as

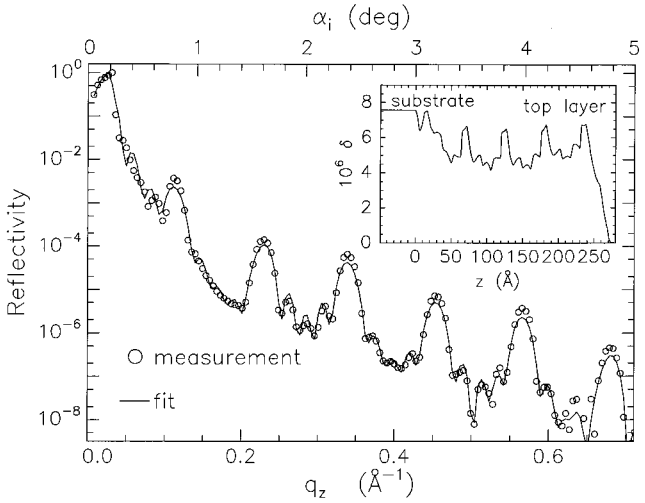

FIG. 5. True specular reflectivity (symbols) and the best fit (line) of the CdA LB film with nine layers obtained at the rotating anode laboratory source with a wavelength of $\lambda = 1.54$ Å. The inset shows the corresponding dispersion profile $\delta(z)$. The peaks indicate the locations of the Cd bilayers.

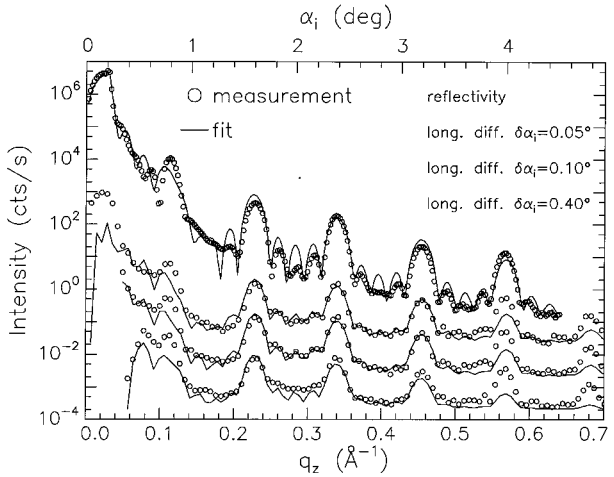

FIG. 6. Total reflectivity (specular and diffuse) and three longitudinal diffuse scans for different offsets $\delta\alpha_i = 0.05°$, 0.10°, 0.40° for the nine-layer CdA LB film. The measurements (symbols) were performed with a rotating anode and the best fit is given by the solid lines. For clarity all curves are shifted down by one order of magnitude on the intensity scale.

discussed above. An arbitrary density profile was sliced into very thin layers of uniform density and the true specular intensity was calculated using the formulas of Sec. II A. The Cd bilayers (highest electron densities) as well as the single Cd layer on the substrate can be clearly seen. Furthermore the density profile reveals that there is a certain amount of disorder in this LB film because the (vertical) structure of the hydrocarbon chains differs slightly from bilayer to bilayer. With a completely regular structure a fit of this quality was not achieved (see below). Particularly the damped modulations in the vicinity of the first Bragg peak of the LB film cannot be explained with a more perfect layer structure of the sample.

More detailed information about the interfaces was obtained by measurements and fits of the diffuse scattering. The symbols in Fig. 6 show the reflectivity[61] as well as three longitudinal diffuse scans with different offsets $\delta\alpha_i = 0.05°$, 0.10°, 0.40°. Figures 7 and 8 show three detector scans with fixed incidence angles $\alpha_i = 0.20°$, 0.80°, 1.60° and eight rocking curves (transverse scans) within the region $0.050 \leqslant q_z \leqslant 0.229$ Å^{-1}.

With the above explained regular slab model the fits (solid lines) in Figs. 6–8 were obtained. The results for the interface and layer parameters are given in Table I. Figure 4(a) shows a sketch of the assumed vertical structure of this sample. The numbers (1) to (6) represent the different interfaces. Note that the top and bottom of the thin Cd bilayer interfaces are assumed to be perfectly conformal, i.e., the interface parameters are the same. Also a low-density region between adjacent hydrocarbon layers does not improve the quality of the fits [Figs. 4(a) and 4(b)]. Because of the assumed regular layer structure there are some deviations between the fit and the measured reflectivity in Fig. 6. But the reflectivity (strictly speaking the true specular plus diffuse intensity at $q_x = 0$) is only one curve in a rather large set of data and the aim is a good simultaneous fit of *all* curves. Furthermore a theory that correctly takes into account the diffuse scattering of a density profile as given in the inset of Fig. 5, is too complex for an effective χ^2 minimizing computer program.[62]

The structure of the three longitudinal diffuse scans in Fig. 6 is well reproduced by the fits. Their pronounced modulations indicate strong vertical correlations between the roughnesses of the different layers. This is supported by a mean value of $\xi_\perp = 700$ Å [model (i) in Sec. II C, see Eq. (5)]. Since this value is 3 times larger than the total LB film thickness of $d = 251$ Å the vertical roughness correlations are rather perfect. The deviations between the fits and the measurement for very small q_z values stem from a background caused by the primary beam. The modulation amplitudes and periods are nearly independent from the chosen offset angle $\delta\alpha_i$. This indicates that shorter wavelengths ($\approx$2000 Å) of the roughness spectrum seem to be transferred in a nearly

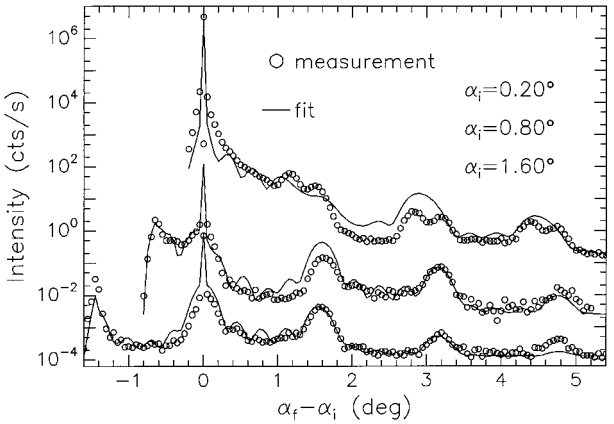

FIG. 7. Detector scans for three different incidence angles $\alpha_i = 0.20°$, 0.80°, 1.60° for the nine-layer CdA sample. The measurements are given by the symbols and the best fit is given by the solid lines. For clarity all curves are displaced with respect to one another by one order of magnitude on the intensity scale.

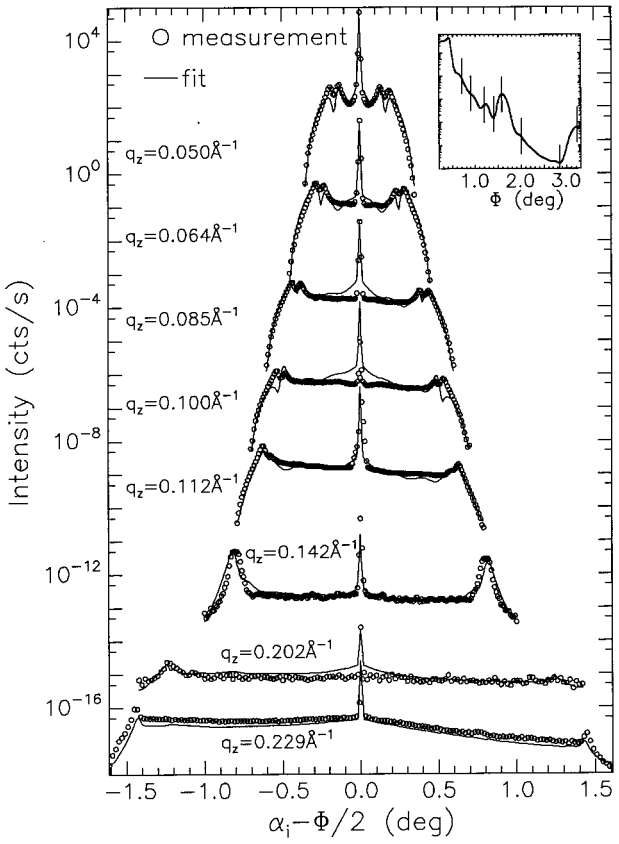

FIG. 8. Transverse scans at different q_z positions for the nine-layer CdA sample. The measurements are given by the symbols and the best fit is given by the solid lines. For clarity all curves are displaced with respect to one another by one order of magnitude on the intensity scale. The inset shows the first part of the reflectivity. The vertical lines mark the positions where the transverse scans were taken.

undamped fashion from the bottom to the top through the whole LB film[39] and supports the assumption of a frequency independent vertical correlation parameter $\xi_\perp$.

The detector scans shown in Fig. 7 are also explained satisfactorily. Only the scan with the incidence angle $\alpha_i = 0.20°$ shows significant deviations between measurement and fit. This incidence angle is less than the critical angle of the Cd-Cd layers and less than the critical angle of bulk Si. Therefore, the penetration depth of the x rays is rather small and the scattered intensity mainly stems from the topmost layers. In this region the difference between our simplified slab model and the density profile obtained from the true specular data (see inset of Fig. 5) is remarkable. Therefore these deviations between fit and measurement are not surprising. For larger angles of incidence the calculation yields very good fits. The same statement holds for the eight transverse scans that are shown in Fig. 8. The larger the q_z value the better the agreement between measurement and fit. The vertical lines in the inset of Fig. 8 indicate the q_z locations of the scans.

One can see that the slab model is able to explain the whole data set quantitatively. The observed deviations between measurement and fit are caused by oversimplifications in the model. Since the introduction of intermediate regions

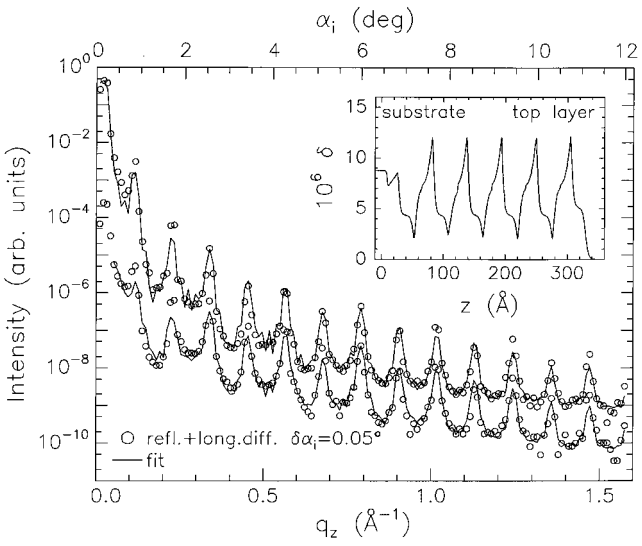

FIG. 9. Total reflectivity (specular plus diffuse) and a longitudinal diffuse scan with offset $\delta\alpha_i = 0.05°$ for the 11-layer CdA LB film. The measurements (symbols) were performed at the wiggler beamline W1 at HASYLAB and the best fit is given by the solid lines. For clarity the curves are shifted by one order of magnitude on the intensity scale. The inset shows the corresponding $\delta(z)$ profile with the narrow Cd peaks.

of very low density between adjacent hydrocarbon chains did not improve the fit for this sample, we believe that the discrepancies do not result from the decomposition of each CdA layer into only two boxes, but rather from the assumption of equal densities for all CdA head groups and hydrocarbon chains, instead of a more realistic density profile as indicated in the inset of Fig. 5.

2. LB film with 11 layers

The second sample, a LB film with 11 layers CdA, was measured using the surface x-ray scattering diffractometer at the W1 beamline at HASYLAB (see Sec. IV A).

Figure 9 shows the total reflectivity (specular plus diffuse) together with a longitudinal diffuse scan with angular offset $\delta\alpha_i = 0.05°$. Note that for clarity the longitudinal diffuse scan is displaced by one order of magnitude on the intensity scale. Again in a wide range (here $q_z > 0.53$ Å^{-1}) the reflected intensity is purely diffuse and the oscillations indicate strong vertical roughness correlations. Because the measurements were done at a synchrotron radiation source it was possible to perform transverse diffuse scans (rocking curves) for rather large q_z values. Figure 10 shows three rocking curves for $q_z = 0.331$, 0.402, and 0.792 Å^{-1}. Whereas in the lower two curves a narrow, resolution limited specular peak is visible, the curve at $q_z = 0.792$ Å^{-1} shows only a broad diffuse maximum.[63]

Due to the large region in reciprocal space that is covered by the scans we have used the kinematical approximation in the calculations. The fit is given by the solid lines in Figs. 9 and 10. Of course they cannot explain the regions where dynamical effects dominate the scattering, i.e., the regions of very small q_z values and the regions of very small incidence and exit angles, respectively. Another consequence of the rather large momentum transfer is that the calculations are

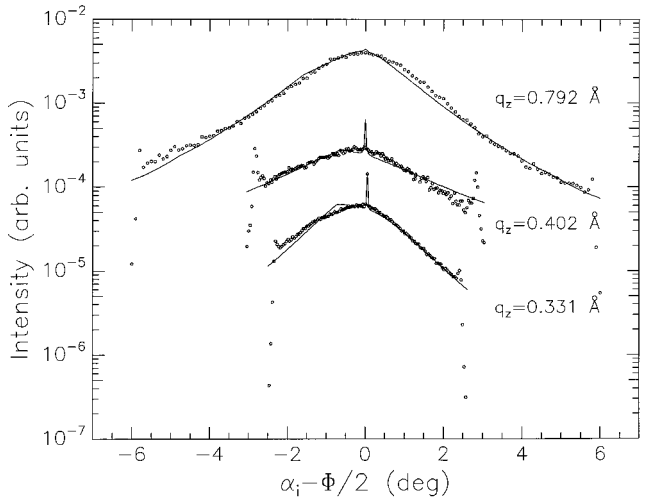

FIG. 10. Three transverse scans at rather large q_z positions for the 11-layer CdA sample. The measurements are given by the symbols and the best fit is given by the solid lines. For clarity all curves are displaced with respect to one another by one order of magnitude on the intensity scale. Note that the asymmetry of the curves only is caused by the scattering geometry.

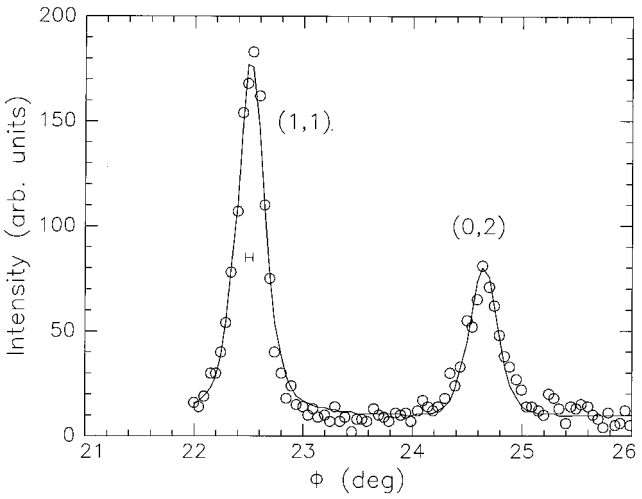

FIG. 11. (1,1) and (0,2) GID reflections of the 11-layer CdA sample. The small horizontal line shows the instrumental resolution. The solid lines are Gaussians that were fitted to the data (symbols) to obtain accurate values for the peak widths.

now more sensitive to the very thin intermediate regions of low density as shown in Fig. 4(b) [interfaces (a)–(e)]. Table II gives the results for the interface parameters obtained from the best fit to the measurements. Since there was almost no evolution of the (lateral) roughness within the 9-layer LB film the fit was obtained by assuming the same ξ_j and h_j values for all LB interfaces and using model (ii) of Sec. II C for the roughness correlations.

Again the calculations are able to explain the data quantitatively. The parameter $\xi_\perp = 9000$ Å is much larger than the total layer thickness, indicating strong vertical correlations of the roughnesses within the 11-layer LB film too. Note that no correlation between the substrate roughness and the LB interfaces was assumed. The inset of Fig. 9 shows the resultant density profile. Although the strong diffuse scattering signal for large q_z values is a proof of a certain amount of disorder in the film, the distance of the main Bragg peaks in the reflectivity corresponds to the Cd-Cd distance of 55 Å, i.e., the thickness of one bilayer of *Y*-type CdA.

3. GID experiments

To investigate the crystalline structure of the 11-layer LB sample, GID experiments were performed. In Fig. 11 a high-resolution measurement of the two strongest GID reflections can be seen. They were obtained by integrating over a region of $\Delta q_z = 0.22$ Å^{-1} along rods perpendicular to the surface and they were identified as the (1,1) and (0,2) reflections of an orthorhombic unit cell with lattice vectors $a_{(10)} = 5.01$ Å and $a_{(01)} = 7.81$ Å. Weak higher-order reflections at $q_r = 2.05$ Å^{-1} and $q_r = 2.51$ Å^{-1} [$q_r = 2k_i \sin(\phi/2)$ is the GID momentum transfer] were also observed [(1,2) and (2,0) reflections]. It is well known from other experiments that this orthorhombic in-plane order on Si substrates exists [see atomic force microscopy (AFM) experiments by Schwartz *et al.*[64] and the diffraction measurements by Tippmann-Krayer[65]] whereas CdA LB films on water show a hexagonal structure.[53,54] We were mainly interested in the spatial extent $L_\parallel$ of the ordered regions of our layer system. Therefore the GID experiment was performed with rather high resolution δ_ϕ. Two Gaussians with full width at half maximum η were fitted to the reflections of Fig. 11 and the broadening of these peaks can be calculated via $\eta_\parallel = (\eta^2 - \eta_{\rm res}^2)^{1/2}$ with the known resolution $\eta_{\rm res}$ of the diffractometer. The fit yields $\eta_\parallel = 0.315° \pm 0.008°$. Using the Scherrer equation[66]

$$L_\parallel = \frac{0.94\lambda}{\cos(\phi/2)} \frac{1}{\eta_\parallel}$$

with $\lambda = 1.659$ Å and the GID scattering angle ϕ of the respective reflection leads to a value of $L_\parallel = 265$ Å for the width of the laterally ordered regions. To investigate the crystallinity perpendicular to the surface, Bragg rods along q_z at the positions of the (1,1) and (0,2) reflections were measured. The (111) and (113) reflections were found as weak modulations of the Bragg rod of the (110) reflection. From the width $\eta_\perp$ of the (113) reflection ($\eta_\perp = 2.15°$) a value of $L_\perp = 42$ Å for the size of the crystalline ordered regions in the z direction is obtained. This is smaller than the thickness of one bilayer and again indicates that the disorder in the structure of this system is concentrated in the z direction perpendicular to the surface.

C. Discussion and conclusions

Tables I and II give the parameters that are obtained for the two samples. For the Si substrates $\delta_{\rm Si} = 7.56 \times 10^{-6}$ ($\lambda = 1.54$ Å) and $\delta_{\rm Si} = 8.79 \times 10^{-6}$ ($\lambda = 1.659$ Å) (Ref. 67) and $\xi_{\rm Si} = 1000$ Å, and $h_{\rm Si} = 0.5$ were assumed. The calculations are rather insensitive to variations of the substrate parameters $h_{\rm Si}$ and $\xi_{\rm Si}$ and therefore realistic values were used. The densities of the Cd layers are always significantly lower than the value given in the literature[67] ($\delta_{\rm Cd} \approx 8 \times 10^{-6}$ compared to the literature value of $\delta_{\rm Cd} \approx 20 \times 10^{-6}$ for $\lambda = 1.54$ Å) whereas the densities of the chains are not quite different from the known values ($\delta_{\rm chain} \approx 3.0 \times 10^{-6}$ compared to $\delta_{\rm chain} \approx 3.5 \times 10^{-6}$ from textbooks). The reason for the discrepancy between the mea-

sured dispersions for the Cd layers in our films and the ideal value is that these Cd bilayers are very thin ($\approx$5 Å) and the density contrast to the hydrocarbon chains is rather large, which yields narrow peaks in the δ profile. Therefore even the small observed roughnesses of only $\sigma\approx$3 Å tend to smear out the profile and lead to a decrease of the average electron densities of the Cd layers by about a factor of 2. Furthermore Tables I and II reveal that the roughnesses of the Cd/CH chain interfaces are considerably smaller than the roughnesses of the CH-chain/air and intermediate layer interfaces.[68,69]

To get a structural model of the interfaces of our CdA LB films we have to discuss several possibilities. First of all our measurements rule out a rather regular island formation on top of the last layer as observed by AFM measurements of other groups.[64,70] Maybe the reason is that these authors have used other substrates and other preparation conditions. We can definitely exclude an island formation. Islands of the same material on top of a layer system would yield a longitudinal diffuse scattering signal that is *out of phase* with the specularly reflected intensity[29,71] quite similar to the intensity that is scattered from a surface grating in nonspecular directions.[72,73] Furthermore no evidence for a regular structure on the topmost surface is found in the transverse scans. A nearly periodic structure would yield at least broad first-order satellite peaks lying under the diffuse scattering stemming from the random roughness.[74] But for both samples the observed behavior clearly shows that the longitudinal diffuse scattering is *in phase* with the specular intensity and *no* indications for satellites are found in any of the transverse scans (see Figs. 6, 8, 9, and 10). This means that the diffuse scattering is caused by random roughness and not by a formation of a rather regular island arrangement.

The most prominent feature in the diffuse scattering experiments is the strong vertical correlation of the roughnesses of the interfaces in both samples ($\xi_\perp$=700 and 9000 Å). Although the differences of the substrate roughness were quite large (σ_{oxid}=3 and 12 Å, respectively; Sec. III) the structures of both organic multilayers are very similar. This can only be explained if already the first transferred CdA layer very effectively damps the substrate roughness. This means that the first layer prevents a propagation of the oxide roughness into the LB film. Therefore the observed strong vertical correlations in both films ($d_{\text{LB film}}$) stem from the replication of roughness of the various LB interfaces. The calculations reveal that the source of the conformal roughness is the first LB layer, i.e., the layer that has smoothed the substrate, which seems to contain a certain amount of holes or defects. Vertical roughness correlations in LB films were also found by Barberka *et al.*[75] But in contrast to our measurements for CdA with perfect roughnesses correlations of *all* LB interfaces, their measurements for Cd stearate yield a restriction of vertical correlations to less than three bilayers.

The strong vertical correlations together with the obtained density profiles (see insets of Figs. 5 and 9) show that there is nearly no crystalline order in the z direction. Additionally the small value of $L_\perp$=42 Å that is obtained from the analysis of the Bragg rods along q_z (see Sec. V B) is an independent hint that the crystalline order in these films is purely two dimensional. Note that this does not mean that the layer structure itself is absent. The sharp Bragg peaks that are observed in the reflectivity of both samples indicate that the bilayer spacing of 55 Å is unaffected. However, this layer structure seems to be perturbed by holes and other defects, which cause a conformal transfer of the roughness from one layer to the next as shown in Fig. 12. As already mentioned, the high degree of vertical correlations can only be explained if these defects are assumed to be already present in the first CdA layer. Apparently the preparation of this first layer is crucial for a homogeneous well-ordered film structure because no tendency of smoothing holes and other imperfections within the organic multilayer stack was obtained from the explanation of the data of the 9-layer sample. Although the fit results show a weak tendency of smoothing the lateral ''jaggedness'' from h_6=0.25 (strongly jagged interface) at the bottom to h_2=0.5 (less jagged interface) at the top of the film, the error bars for this parameter are large. The vertical rms roughnesses of the LB interfaces show *no* significant smoothing with increasing layer number.

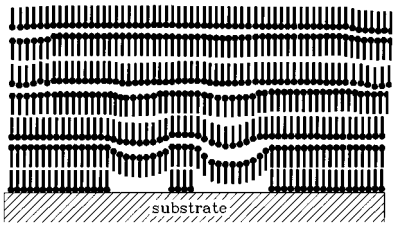

FIG. 12. Sketch of the defect structure of the investigated LB films. Because of defects strong vertical roughness correlations occur and the crystalline order in the z direction is strongly perturbed. Note that the Cd-Cd distance is nearly unaffected by these perturbations.

We have chosen a self-affine fractal model for the description of the interface structures (see Sec. III C). Gibaud *et al.*[9] explain their data with a roughness exponent of h=0.5 and assuming no lateral cutoff ξ, i.e., $\xi=\infty$ (or at least a ξ that is larger than the spatial extent of the coherently illuminated surface area, i.e., larger than several tens of micrometers). Whereas our results for the 9-layer film also yield h=0.5 for the topmost surface we cannot confirm this value for the 11-layer LB film. The major difference between our analysis and that of Gibaud *et al.*[9] is that we have used a full scattering theory for the explanation of our data whereas Gibaud *et al.* model the scattering of the whole layer stack by the scattering from a single interface. Therefore our fit results are much more sensitive to the individual roughness parameters, particularly to ξ and h. The value of h=0.77 for the 11-layer CdA LB film shows a less jagged surface compared to the result for the first sample. However, this number is an average over the whole film because the h values of individual interfaces were not varied in the fit. The additional bilayer may yield a surface that is less jagged than the interface below because the 9-layer sample shows the weak trend that h slightly increases with the number of bilayers. Also the assumption of $\xi=\infty$ is not confirmed by our measurements. For the 9-layer sample we found a value of $\xi\approx$350 Å for all interfaces with no remarkable tendency from the bottom to the top of the film, which is consistent with the strong vertical roughness correlations. This means that the lateral correlation length ξ seems to be unaffected by the layer by layer

LB preparation technique. The second sample yields a slightly smaller value of $\xi=235$ Å for the cutoff length. Taking into account the error bars of approximately 100 Å that were obtained for the first sample, a value of $\xi\approx300$ Å seems to be typical for CdA layer systems.[76] This is a rather short length scale and much smaller than the coherence length of the incident beam.

The size of the laterally ordered (crystalline) regions was determined from the GID measurements to be $L_{\|}=265$ Å. This is in agreement with the value obtained for ξ from the diffuse scattering data. It should be clearly mentioned that the parameter ξ does *not* have the meaning of a domain size in the fractal model ξ only corresponds to the domain size if a regular arrangement is assumed. Transferring this situation to a layer consisting of two-dimensional crystalline domains that are present at the interfaces too may lead to the conclusion that ξ now corresponds to the mean size of the domains. Note that the domains that are discussed here are different from the island structure, which was ruled out before.

From the length of the orthorhombic lattice vectors and the obtained value of $L_{\|}$ or ξ we calculate that approximately 40×40 CdA molecules are ordered in small domains within the layers. Their size is comparable with AFM measurements of Chi *et al.*[77] who found domains of $\xi\sim100$ Å on top of fatty acid multilayers.

In general we can say that our experiments confirm the basic result of Gibaud *et al.*[9] who were able to explain their data assuming self-affine rough surfaces within LB films. Although our values for h and particularly for ξ are quite different, the fractal correlation function model is indeed applicable. It should be noted that all fits of the diffuse scattering for one sample are obtained with models that do not have very many parameters compared with the number of data points and the degree of complexity of the obtained curves. Therefore we conclude from the quality of the fits and the comparison with the results of the GID experiments that we can describe the interfaces of our investigated LB films with the self-affine fractal model. On one hand this is surprising because this form of a correlation function is typical for the growth of semiconductor and metal surfaces. On the other hand the LB film preparation technique may lead to a statistically rough interface because the long hydrocarbon chains that are oriented in the z direction may be slightly tilted in random directions, yielding slightly different heights of the molecules of the next layer. Because the projected length of one molecule depends on the cosine of the tilt angle this does not affect the observed average layer thickness unless the tilt becomes rather large.

VI. SUMMARY AND OUTLOOK

In summary, we have presented a detailed characterization of the interface structure of CdA LB films with x-ray scattering experiments. The combination of GID investigations and measurements in the region of total external reflection yields a consistent picture of the samples. The interfaces are found to be self-affine rough with a rather small correlation length of $\xi\approx300$ Å, which is in the same range as the domain size $L_{\|}$ of the two-dimensional crystalline structure. Furthermore a very high degree of conformal roughness was detected. Since the two substrates have rather different roughnesses and the structures of both films are indeed quite similar, we can rule out that the source of this conformality is simply a replication of substrate roughness. This leads us to suspect that defects within the first organic layer are decisive. They were transferred in a nearly undamped manner throughout the whole LB stacks. The quality of the organic multilayer seems to depend strongly on the quality of the first prepared layer on the Si substrate. There is no healing mechanism at room temperature that smooths defects or holes within CdA LB films. However, we found that one CdA layer is able to damp very effectively a rather rough substrate morphology.

In future work, a systematic temperature-dependent diffuse x-ray scattering study of LB films would be of interest because it might be possible to heal most of the defects by a subsequent annealing of the film. These experiments together with the analysis technique presented in this paper would provide a better understanding of the growth mechanism and the defect structure of LB films on solid substrates.

ACKNOWLEDGMENTS

The authors would like to thank A. Doerr and L. Schwalowsky for fruitful discussions. One of us (V. N.) was partly supported by the Deutsche Forschungsgemeinschaft under Contract No. Pr325-1.

[1] V. K. Agarwal, Phys. Today **41** (6), 40 (1988).
[2] H. Fuchs, H. Ohst, and W. Prass, Adv. Mater. **3**, 10 (1991).
[3] M. Stelzle, Ph.D. thesis, TU München, 1992.
[4] K. B. Blodgett and I. Langmuir, Phys. Rev. **51**, 964 (1937).
[5] J. Als-Nielsen, D. Jacquemain, K. Kjaer, F. Leveiller, M. Lahav, and L. Leiserowitz, Phys. Rep. **246**, 251 (1994).
[6] R. Stömmer, J. Grenzer, J. Fischer, and U. Pietsch, J. Phys. D **28**, A216 (1995).
[7] R. Stömmer, U. English, U. Pietsch, and V. Holý, Physica B (to be published).
[8] Z. Li, W. Zhao, J. Quinn, M. H. Rafailovich, J. Sokolov, R. B. Lennox, A. Eisenberg, X. Z. Wu, M. W. Kim, S. K. Sinha, and M. Tolan, Langmuir **11**, 4785 (1995).
[9] A. Gibaud, N. Cowlam, G. Vignaud, and T. Richardson, Phys. Rev. Lett. **74**, 3205 (1995).
[10] L. G. Parratt, Phys. Rev. **95**, 359 (1954).
[11] F. Abelés, Ann. Phys. (Paris) **5**, 596 (1950).
[12] L. Névot and P. Croce, Rev. Phys. Appl. **15**, 761 (1980).
[13] J. Lekner, *Theory of Reflection* (Martinus Nijhoff, Dordrecht, 1987).
[14] H. Dosch, *Critical Phenomena at Surfaces and Interfaces (Evanescent X-Ray and Neutron Scattering)*, Springer Tracts in Modern Physics Vol. 126 (Springer-Verlag, Berlin, 1992).
[15] R. W. James, *The Optical Principles of the Diffraction of X-Rays*

(Ox Bow Press, Woodbridge, 1982).
[16] S. K. Sinha, E. B. Sirota, S. Garoff, and H. B. Stanley, Phys. Rev. B **38**, 2297 (1988).
[17] R. Pynn, Phys. Rev. B **45**, 602 (1992).
[18] D. K. G. de Boer, Phys. Rev. B **49**, 5817 (1994).
[19] V. Holý, J. Kuběna, I. Ohlídal, K. Lischka, and W. Plotz, Phys. Rev. B **47**, 15 896 (1993).
[20] V. Holý and T. Baumbach, Phys. Rev. B **49**, 10 668 (1994).
[21] J.-P. Schlomka, M. Tolan, L. Schwalowsky, O. H. Seeck, J. Stettner, and W. Press, Phys. Rev. B **51**, 2311 (1995).
[22] J.-P. Schlomka, M. R. Fitzsimmons, R. Pynn, J. Stettner, O. H. Seeck, M. Tolan, and W. Press, Physica B (to be published).
[23] J. Stettner, L. Schwalowsky, O. H. Seeck, M. Tolan, W. Press, C. Schwarz, and H. v. Känel, Phys. Rev. B **53**, 1398 (1996).
[24] M. Born and E. Wolf, *Principles of Optics* (Pergamon, Oxford, 1964), 2nd (revised) ed.
[25] J. Lekner, Physica B **173**, 99 (1991).
[26] A. V. Andreev, A. G. Michette, and A. Renwick, J. Mod. Opt. **35**, 1667 (1988).
[27] W. A. Hamilton and R. Pynn, Physica B **173**, 71 (1991).
[28] D. Bahr, W. Press, R. Jebasinski, and S. Mantl, Phys. Rev. B **47**, 4385 (1993).
[29] S. K. Sinha, J. Phys. (France) III **4**, 1543 (1994).
[30] R. Chiarello, V. Panella, J. Krim, and C. Thompson, Phys. Rev. Lett. **67**, 3408 (1991).
[31] G. Palasantzas, Phys. Rev. B **48**, 14 472 (1993).
[32] G. Palasantzas, Phys. Rev. B **49**, 10 544 (1994).
[33] Z. H. Ming, A. Krol, Y. L. Soo, Y. H. Kao, J. S. Park, and K. L. Wang, Phys. Rev. B **47**, 16 373 (1993).
[34] B. B. Mandelbrot, *The Fractal Geometry of Nature* (Freeman, New York, 1982).
[35] M. F. Barnsley, R. L. Devaney, B. B. Mandelbrot, H.-O. Peitgen, D. Saupe, and R. F. Voss, *The Science of Fractal Images* (Springer-Verlag, New York, 1988).
[36] H.-O. Peitgen, H. Jürgens, and D. Saupe, *Bausteine des Chaos-Fraktale* (Springer-Verlag, Berlin, 1992).
[37] L. Feigin and I. I. Samoilenko, Physica B **198**, 116 (1994).
[38] T. Salditt, T. H. Metzger, and J. Peisl, Phys. Rev. Lett. **73**, 2228 (1994).
[39] E. E. Fullerton, J. Pearson, C. H. Sowers, S. D. Bader, X. Z. Wu, and S. K. Sinha, Phys. Rev. B **48**, 17 432 (1993).
[40] M. K. Sanyal, S. K. Sinha, A. Gibaud, S. K. Satija, C. F. Majkrzak, and H. Homma, in *Surface X-Ray and Neutron Scattering*, edited by H. Zabel and I. K. Robinson, Springer Proceedings in Physics Vol. 61 (Springer-Verlag, Berlin, 1992), pp. 91–94.
[41] S. K. Sinha, M. K. Sanyal, S. K. Satija, C. F. Majkrzak, D. A. Neumann, H. Homma, S. Szpala, A. Gibaud, and H. Morkoc, Physica B **198**, 72 (1994).
[42] C. Thompson, G. Palasantzas, Y. P. Feng, S. K. Sinha, and J. Krim, Phys. Rev. B **49**, 4902 (1994).
[43] D. E. Savage, N. Schimke, Y.-H. Phang, and M. G. Lagally, J. Appl. Phys. **71**, 3283 (1992).
[44] Y.-H. Phang, R. Kariotis, D. E. Savage, and M. G. Lagally, J. Appl. Phys. **72**, 4627 (1992).
[45] D. E. Savage, Y.-H. Phang, J. J. Rownd, J. F. MacKay, and M. G. Lagally, J. Appl. Phys. **74**, 6158 (1993).
[46] M. R. Fitzsimmons and E. Burkel, Phys. Rev. B **47**, 8436 (1993).
[47] J. B. Kortright, J. Appl. Phys. **70**, 3620 (1991).
[48] D. G. Stearns, J. Appl. Phys. **71**, 4286 (1992).
[49] E. Spiller, D. Stearns, and M. Krumrey, J. Appl. Phys. **74**, 107 (1993).
[50] A frequency dependence of the vertical correlations would lead to a decrease in the diffuse scattering oscillations in the q_z direction for larger q_x values. Within the accessible q_x region that behavior was not found and the description with a frequency-independent $\xi_\perp$ is allowed.
[51] V. Nitz, Ph.D. thesis, Kiel University, 1995.
[52] C. A. Helm, H. Möhwald, K. Kjaer, and J. Als-Nielsen, Biophys. J. **52**, 381 (1987).
[53] K. Kjaer, J. Als-Nielsen, C. A. Helm, P. Tippmann-Krayer, and H. Möhwald, Thin Solid Films **159**, 17 (1988).
[54] F. Leveiller, D. Jacquemann, M. Lahav, L. Leiserowitz, M. Deutsch, K. Kjaer, and J. Als-Nielsen, Science **252**, 1532 (1991).
[55] L. Wilhelmy, Ann. Phys. (Leipzig) **119**, 177 (1863).
[56] G. L. Gaines, *Insoluble Monolayers on Liquid-Gas Interfaces* (Wiley, New York, 1966).
[57] L. Brügemann, R. Bloch, W. Press, and P. Gerlach, J. Phys. C **2**, 8869 (1990).
[58] L. Brügemann, R. Bloch, W. Press, and M. Tolan, Acta Crystallogr. A **48**, 688 (1992).
[59] R. Feidenhans'l, Surf. Sci. Rep. **10**, 105 (1989).
[60] M. Kardar, G. Parisi, and Y. Zang, Phys. Rev. Lett. **56**, 889 (1986).
[61] Very small differences between the reflectivities of Fig. 5 and Fig. 6 can be seen. Despite the fact that one curve is the true specular intensity and the other the whole reflectivity (true specular plus diffuse at $q_x=0$), both curves are different measurements that were performed on the same sample. Therefore the small deviations between the curves reveal the experimental errors.
[62] S. Dietrich and A. Haase, Phys. Rep. **260**, 1 (1995).
[63] Although the resultant formulas for the diffuse scattering cross section are symmetric concerning the incident and exit angles, the measured transverse scans are asymmetric. The reason is that the illuminated area and the area of the sample that is seen by the detector are functions of these angles. Therefore, Eq. (2) has to be multiplied by two factors, taking into account the geometry and leading to an asymmetry and particularly at large q_z values to ''kinks'' in the calculated curves (for details see Ref. 51).
[64] D. K. Schwartz, J. Garnaes, R. Viswanathan, and J. A. N. Zasazinski, Science **257**, 508 (1992).
[65] P. Tippmann-Krayer, Ph.D. thesis, Mainz University, 1991.
[66] B. E. Warren, *X-Ray Diffraction* (Addison-Wesley, Reading, MA, 1969).
[67] *International Tables for X-Ray Crystallography* (Kynoch Press, Birmingham, 1974).
[68] U. Pietsch, U. Höhne, and H. Möhwald, Langmuir **9**, 208 (1993).
[69] U. Pietsch, T. Barberka, W. Mahler, and T. H. Metzger, Thin Solid Films **247**, 230 (1994).
[70] G. Dreisigacker, Physik. Blätter **1**, 12 (1993).
[71] S. K. Satija, S. K. Sinha, E. B. Sirota, G. J. Hughes, and T. P. Russell (unpublished).
[72] M. Tolan, G. König, L. Brügemann, W. Press, F. Brinkop, and J. P. Kotthaus, Europhys. Lett. **20**, 223 (1992).
[73] M. Tolan, W. Press, F. Brinkop, and J. P. Kotthaus, J. Appl. Phys. **75**, 7761 (1994).
[74] A. Gibaud, R. A. Cowley, D. F. McMorrow, R. C. C. Ward, and

M. R. Wells, Phys. Rev. B **48**, 14 463 (1993).
[75] T. Barberka, U. Höhne, U. Pietsch, and T. H. Metzger, Thin Solid Films **244**, 1061 (1994).
[76] We found the value of $\xi \approx 300$ Å in rather perfect CdA LB films too (Ref. 51). Therefore the magnitude of ξ seems to be independent of the degree of disorder in the films.
[77] L. F. Chi, M. Anders, H. Fuchs, R. R. Johnston, and H. Ringsdorf, Science **259**, 213 (1993).